Arteriosclerosis, Thrombosis, and Vascular Biology

JOURNAL OF THE AMERICAN HEART ASSOCIATION

American Heart Association®

Learn and Live℠

18F-Choline Images Murine Atherosclerotic Plaques Ex Vivo

Christian M. Matter, Matthias T. Wyss, Patricia Meier, Nicolas Späth, Tobias von Lukowicz, Christine Lohmann, Bruno Weber, Ana Ramirez de Molina, Juan Carlos Lacal, Simon M. Ametamey, Gustav K. von Schulthess, Thomas F. Lüscher, Philipp A. Kaufmann and Alfred Buck

Arterioscler Thromb Vasc Biol 2006;26;584-589; originally published online Dec 15, 2005;

DOI: 10.1161/01.ATV.0000200106.34016.18

Arteriosclerosis, Thrombosis, and Vascular Biology is published by the American Heart Association. 7272 Greenville Avenue, Dallas, TX 72514

 Print ISSN: 1079-5642. Online ISSN: 1524-4636

^{18}F-Choline Images Murine Atherosclerotic Plaques Ex Vivo

Christian M. Matter, Matthias T. Wyss, Patricia Meier, Nicolas Späth, Tobias von Lukowicz, Christine Lohmann, Bruno Weber, Ana Ramirez de Molina, Juan Carlos Lacal, Simon M. Ametamey, Gustav K. von Schulthess, Thomas F. Lüscher, Philipp A. Kaufmann, Alfred Buck

Objective—Current imaging modalities of atherosclerosis mainly visualize plaque morphology. Valuable insight into plaque biology was achieved by visualizing enhanced metabolism in plaque-derived macrophages using ^{18}F-fluorodeoxyglucose (^{18}F-FDG). Similarly, enhanced uptake of ^{18}F-fluorocholine (^{18}F-FCH) was associated with macrophages surrounding an abscess. As macrophages are important determinants of plaque vulnerability, we tested ^{18}F-FCH for plaque imaging.

Methods and Results—We injected ^{18}F-FCH (n=5) or ^{18}F-FDG (n=5) intravenously into atherosclerotic apolipoprotein E-deficient mice. En face measurements of aortae isolated 20 minutes after ^{18}F-FCH injections demonstrated an excellent correlation between fat stainings and autoradiographies (r=0.842, P<0.0001), achieving a sensitivity of 84% to detect plaques by ^{18}F-FCH. In contrast, radiotracer uptake 20 minutes after ^{18}F-FDG injections correlated less with en face fat stainings (r=0.261, P<0.05), reaching a sensitivity of 64%. Histological analyses of cross-sections 20 minutes after coinjections of ^{18}F-FCH and ^{14}C-FDG (n=3) showed that ^{18}F-FCH uptake correlated better with fat staining (r=0.740, P<0.0001) and macrophage-positive areas (r=0.740, P<0.0001) than ^{14}C-FDG (fat: r=0.236, P=0.29 and CD68 staining: r=0.352, P=0.11), respectively.

Conclusions—^{18}F-FCH identifies murine plaques better than ^{18}F-FDG using ex vivo imaging. Enhanced ^{18}F-FCH uptake into macrophages may render this tracer a promising candidate for imaging plaques in patients. (***Arterioscler Thromb Vasc Biol*. 2006;26:584-589.**)

Key Words: atherosclerosis ■ macrophages ■ apolipoprotein E knockout mice ■ autoradiography ■ radionuclide

Current clinical tools to image atherosclerotic plaques such as intravascular ultrasound, computed tomography (CT), magnetic resonance imaging (MRI), or optical coherence tomography (OCT) provide morphological images of the vessel wall at remarkable spatial resolution.[1–4] However, these imaging modalities are unable to characterize details of plaque biology. More insight into plaque biology would be desirable to determine a better risk assessment of the vulnerable plaque.[5] The vulnerable plaque, because of its risk of rupturing, is considered the culprit lesion causing acute arterial obstruction, which may result in myocardial infarction or stroke.

Therefore, plaque imaging using molecular targets has gained increased attention.[6] For example, positron emission tomography (PET) provides attractive opportunities to visualize plaque biology.[7] Specifically, ^{18}F-fluorodeoxyglucose (^{18}F-FDG)—a widely used PET tracer—has been clinically used to image enhanced metabolism of cellular components of the plaque including macrophages.[8] Other studies have confirmed the relevance of ^{18}F-FDG for plaque imaging in Watanabe rabbits[9] and in patients with calcifications of the arterial wall[10] or active atherosclerosis.[11] These studies are of interest as macrophages play a crucial role in atherogenesis and, particularly, in plaque rupture.[12,13]

^{18}F-labeled fluorocholine (^{18}F-FCH) has been introduced as a tracer for imaging brain and prostate cancer.[14,15] Choline is taken up into cells by specific transport mechanisms, phosphorylated by choline kinase, metabolized to phosphatidylcholine, and eventually incorporated into the cell membrane.[16–18] Increased choline uptake has been shown in tumor cells[19] and activated macrophages.[17] Based on this concept, we have recently demonstrated an enhanced ^{18}F-FCH uptake that correlated with macrophage accumulation as part of an inflammatory reaction after soft tissue infection[20] or acute cerebral radiation injury.[21]

Original received July 5, 2005; final version accepted November 29, 2005.

From Cardiovascular Research (C.M.M., P.M., T.v.L., C.L., T.F.L.), Institute of Physiology, University of Zurich, Cardiovascular Center, University Hospital Zurich and Center for Integrative Human Physiology (C.M.M., T.v.L., T.F.L., P.A.K.), University of Zurich, and Nuclear Medicine (M.T.W., N.S., B.W., G.K.v.S., A.B.), University Hospital Zurich, Switzerland; Instituto de Investigaciones Biomédicas (A.R.d.M., J.C.L.), CSIC, Madrid, Spain; Center for Radiopharmaceutical Science Paul Scherrer Institute (S.M.A., P.A.K.), Villigen, Switzerland; and Nuclear Cardiology (P.A.K.), University Hospital Zurich, Switzerland.

P.A.K. and A.B. contributed equally to this work.

Correspondence to Christian M. Matter, MD, Cardiovascular Research, Institute of Physiology, Zurich University and CardioVascular Center, University Hospital Zurich, Winterthurerstrasse 190, CH-8057 Zurich, Switzerland. E-mail cmatter@physiol.unizh.ch

Arterioscler Thromb Vasc Biol. **is available at http://www.atvbaha.org** **DOI: 10.1161/01.ATV.0000200106.34016.18**

Therefore, we compared the ability of ^{18}F-FCH and ^{18}F-FDG to image murine atherosclerotic plaques ex vivo and validated these results against fat staining.

Materials and Methods

For more details, please see http://atvb.ahajournals.org.

Animals

Male atherosclerotic apolipoprotein E knockout (*ApoE*$^{-/-}$, C57Bl/6J) mice[22] were fed a high-cholesterol diet (1.25% total cholesterol; RD12108; Research Diets) for 2 months starting at the age of 8 weeks. Animals were kept without food for 4 hours before injections of the radiotracers until sacrifice. A subset of wild-type C57Bl/6J mice without atherosclerosis received a normal chow diet. All animal experiments were performed in accordance with our institutional guidelines and approved by the local animal committee.

Radionuclides

Ex vivo plaque imaging was performed after injections of ^{18}F-FCH (45.8 to 60.5 MBq; n=5), ^{18}F-FDG (36.7 to 46.4 MBq; n=5), or coinjections of ^{18}F-FCH and ^{14}C-FDG (185kBq; n=3) in 300 μL normal saline into the animals' tail veins.

Harvesting and Tissue Processing

For determining the uptake of ^{18}F-FCH, ^{18}F-FDG, or ^{14}C-FDG within plaques, *ApoE*$^{-/-}$ mice were euthanized 20 minutes after injection of the radiotracer(s); additional animals were euthanized 3 hours after ^{18}F-FDG injections. For en face analyses, distal aortae were opened longitudinally. For microscopic examinations, 3 samples of the proximal aorta were embedded in OCT compound (Tissue-Tek, Sakura, the Netherlands) and frozen in isopentane. Serial cross-sections of 10 μm thickness were immediately cut and thaw-mounted on glass slides. Autoradiography and fat stainings were performed on the same samples (n=12 from each animal). For biochemical analyses, aortae from *ApoE*$^{-/-}$ (n=3) and wild-type mice (n=3) were shock-frozen in liquid nitrogen (LN_2) and stored at −80°C.

Choline Kinase Activity and Expression

For more details, please see http://atvb.ahajournals.org.

Plaque Imaging

Morphology

Plaque areas were assessed via fat staining using Oil-red O. Macrophages were identified on adjacent cross-sections using a rat anti-mouse CD68 monoclonal antibody (Serotec, Clone FA-II, 1:400).

Autoradiography

For en face macroautoradiography, aortae were longitudinally opened and exposed on a phosphor imaging screen with ^{14}C standards (for 4 hours with ^{18}F-labeling; for 10d using ^{14}C-labeling). Furthermore, aortic cross-sections of 10 μm thickness were exposed with ^{14}C standards for microautoradiography. The data were scanned (Fuji BAS 1800 II; pixel size, 50 μm) and converted to kBq/cc.

Signal Quantification

The lesion-to-nonlesion ratio in autoradiographies of longitudinally opened aortae was determined using linear integration of signal intensity (NIH Image J 1.33 software) over corresponding aortic areas taking the mean of 5 measurements from each animal. The corresponding ratio in 3 cross-sections of the proximal aorta was determined after injections of ^{18}F-FCH or ^{18}F-FDG by relating the signal intensity of a region of interest within the plaque to a region without lesion. In addition, the standardized uptake value (SUV) was obtained for each animal by dividing the target tissue radioactivity uptake (kBq/cc) within a region of interest by the injected activity per gram of body weight. Comparisons between en face fat stainings and corresponding autoradiographies were determined by converting the autoradiographies into color-coded images, tracing all positive areas (Analysis Five Docu, SoftImaging System) and correlating the percent positive of the total vessel areas using the Spearman rank correlation test (GraphPad Prism V4). Analogous comparisons were performed on 3 cross-sections of each animal in the proximal aorta after coinjections of ^{18}F-FCH and ^{14}C-FDG (n=3) for autoradiographies, fat, and CD68 stainings.

Mouse PET

For more detail, please see http://atvb.ahajournals.org.

Statistics

An unpaired *t* test was used to compare results between different groups. Values are given as mean±SD; $P<0.05$ was considered statistically significant.

Results

^{18}F-FCH Macroscopically Visualizes Murine Atherosclerotic Plaques

En face analysis of atherosclerotic plaques revealed a strong and selective uptake of ^{18}F-FCH (Figure 1A). The mean signal-to-noise ratio of these macroautoradiographies relating radioactivity uptake in plaque-bearing to plaque-free vessel wall was 4.9±2.0 to 1 (n=5). Comparisons of the corresponding en face autoradiographic signals and fat stainings in single plaques demonstrated a highly significant correlation ($r=0.842$, $P<0.0001$) and a sensitivity of 84% to detect fat-stained areas by autoradiography. Because ^{18}F-FCH uptake in rodents and men reaches a plateau 20 minutes after radiotracer injection,[14,15,20,21,23] we did not study further time intervals for plaque imaging using ^{18}F-FCH.

^{18}F-FDG Visualizes Murine Plaques Less Specifically Than ^{18}F-FCH

In light of previous reports with ^{18}F-FDG to image plaque biology in rabbits[9] and patients,[8,10,11] we validated the ability of ^{18}F-FDG to image murine atherosclerotic plaques applying the same experimental protocol as described for ^{18}F-FCH; 20 minutes after injection, ^{18}F-FDG uptake on autoradiography correlated poorly with the fat staining of plaques (Figure 1B, top). The mean signal-to-noise ratio of radioactivity uptake in plaque-bearing versus plaque-free vessel wall was 6.0±5.1 to 1 (n=5). The sensitivity of the autoradiography after ^{18}F-FDG injection was only 64% to detect the fat-stained areas. Comparisons of the corresponding en face autoradiographic signals and fat stainings (Figure 1B) documented a lower correlation ($r=0.261$, $P<0.05$) than for ^{18}F-FCH.

Given the clinical report describing an interval of 3 hours as the optimal time course for ^{18}F-FDG imaging using PET-CT,[8] we investigated whether harvesting aortae 3 hours after intravenous ^{18}F-FDG injections would affect plaque imaging ex vivo. Comparisons between en face autoradiographies and fat stainings 3 hour post radiotracer injections (Figure 1B, bottom; n=3) revealed a slightly better correlation ($r=0.476$, $P<0.001$; Table) than after 20 minutes. However, the mean signal-to-noise ratio of radioactivity uptake in plaque-bearing versus plaque-free vessel wall decreased to 2.6±0.9 to 1 (n=3). In addition, because of a high rate of 76% false-negative autoradiographic signals, the sensitivity of the autoradiography 3 hours after ^{18}F-FDG injection was only 57% to detect the fat-stained areas.

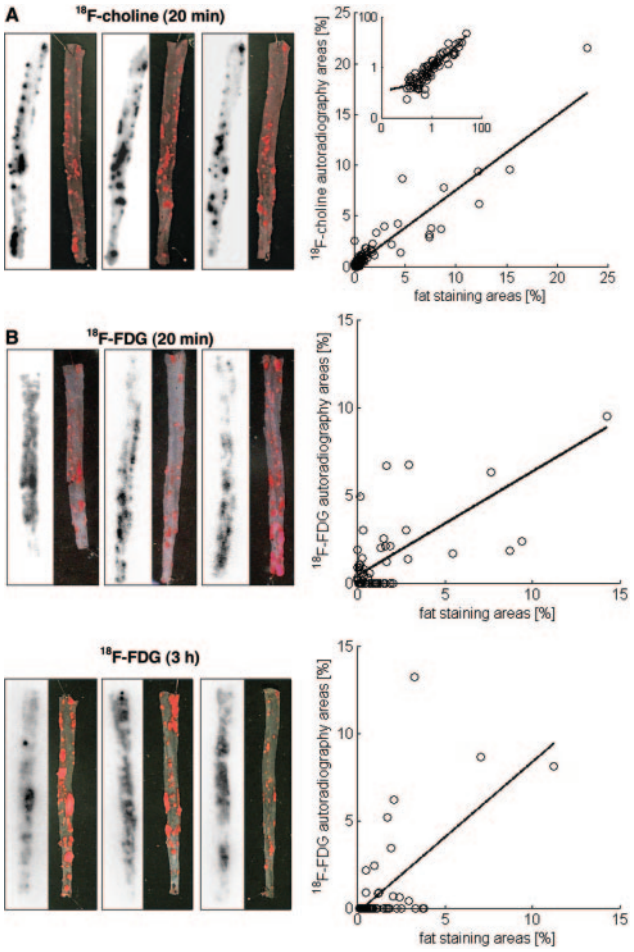

Figure 1. Macroscopically, ^{18}F-fluorocholine (^{18}F-FCH) better visualizes murine plaques than ^{18}F-fluorodeoxyglucose (^{18}F-FDG). A, Macroautoradiographies (left) and fat stainings using Oil-red O (right) of longitudinally opened aortae 20 minutes after injection of ^{18}F-FCH in atherosclerotic apolipoprotein E knockout (*ApoE*$^{-/-}$) mice (3 samples of n=5). Comparisons of corresponding images obtained after autoradiography and fat staining by tracing each positive area (given as % of total vessel area) demonstrate a highly significant correlation (r=0.842, P<0.0001). Each white circle (n=89) refers to a single autoradiographic signal and its corresponding plaque staining. The insert illustrates the same findings on a log scale. B, Macroautoradiographies (left) and fat stainings (right) of aortae 20 minutes (top, 3 samples of n=5) and 3 hours (bottom, n=3) after injection of ^{18}F-FDG in atherosclerotic apolipoprotein E knockout (*ApoE*$^{-/-}$) mice. Comparisons of corresponding images obtained after autoradiography and fat staining by tracing each positive area using linear regression document a poor correlation for ^{18}F-FDG after 20 minutes (r=0.261, P<0.05) and after 3 hours (r=0.476, P<0.001). Each white circle (n=73 for 20 minutes, n=58 for 3 hours) refers to a single autoradiographic signal and its corresponding plaque staining.

^{18}F-FCH Uptake Colocalizes With Plaques Using Microautoradiography

Analyses of cross-sections from the proximal aorta showed that ^{18}F-FCH uptake correlated well with plaques (Figure 2A), whereas ^{18}F-FDG uptake showed a lower sensitivity to identify atherosclerotic plaques (Figure 2B). The maximum of the SUV in the plaque was 1.8±1.0 for ^{18}F-FCH and 2.4±0.5 for ^{18}F-FDG (n=5; not significant [NS]). In addition, the signal-to-noise ratio (plaque-bearing vessel portion to plaque-free vessel wall) was 3.5±0.9 to 1 for ^{18}F-FCH and 2.9±0.5 to 1 for ^{18}F-FDG (NS).

Validation of ^{18}F-FCH or ^{14}C-FDG for Imaging Murine Plaques or Macrophages Ex Vivo in Cross-sections

Radiotracer	^{18}F-FCH	^{14}C-FDG
n (mice)	3	3
n (total plaques analyzed)	22	22
Correlation r (Spearman; tracer vs fat staining)	0.740	0.236
P value (Spearman; tracer vs fat staining)	<0.0001	0.29
Correlation r (Spearman; tracer vs CD68 staining)	0.740	0.352
P value (Spearman; tracer vs CD68 staining)	<0.0001	0.11
SUV	2.5±0.4 to 1	2.4±1.1 to 1
False negative autoradiography for fat staining, %	5	18
Sensitivity of tracer for fat staining, %	95	82
Sensitivity of tracer for CD68 staining, %	96	85

Comparisons of single autoradiographic signals (20 minutes after coinjections of ^{18}F-FCH and ^{14}C-FDG), fat, and CD68 stainings in 3 cross-sections of atherosclerotic aortae; mean±SD.

^{18}F-FCH Uptake Colocalizes With Plaque Macrophages

Autoradiographic analyses of aortic cross-sections after intravenous coinjections of ^{18}F-FCH and ^{14}C-FDG into the same *ApoE*$^{-/-}$ mice showed similar radionuclide uptake in plaque-bearing vessel areas (Figure 3A, top; Table). Under these conditions, the signal-to-noise ratio (lesion to nonlesion) calculated from the SUV was 2.5±0.4 to 1 for ^{18}F-FCH and 2.4±1.1 to 1 for ^{14}C-FDG (n=3; NS).

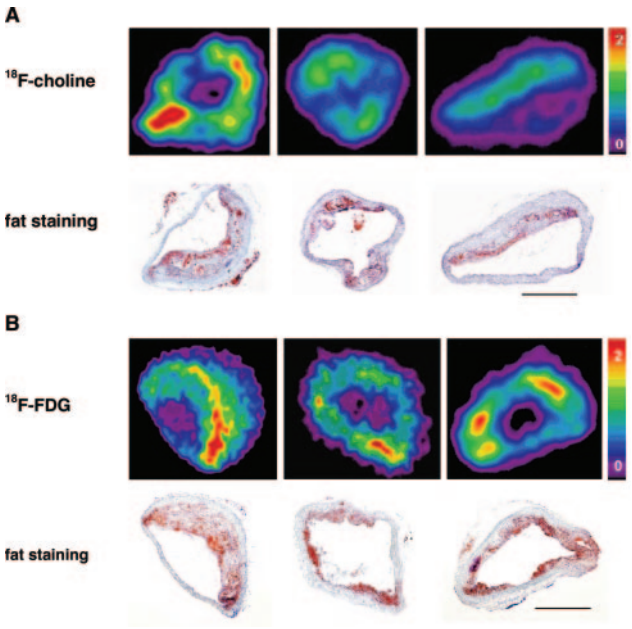

Figure 2. ^{18}F-FCH visualizes atherosclerotic plaques at the microscopic level. Color-coded microautoradiographies (top) and Oil-red O/hematoxyline stainings (bottom) of aortic cross-sections 20 minutes after injection of ^{18}F-FCH (A) (45.8 to 60.5 MBq) or ^{18}F-FDG (B) (36.7 to 46.4 MBq) in apolipoprotein E knockout (*ApoE*$^{-/-}$) mice (n=5). Autoradiographic signals derived from ^{18}F-FCH or ^{18}F-FDG uptake colocalize to a similar degree with fat staining. The color calibration (right) indicates the SUV for ^{18}F-FCH or ^{18}F-FDG, respectively; bar=500 μm.

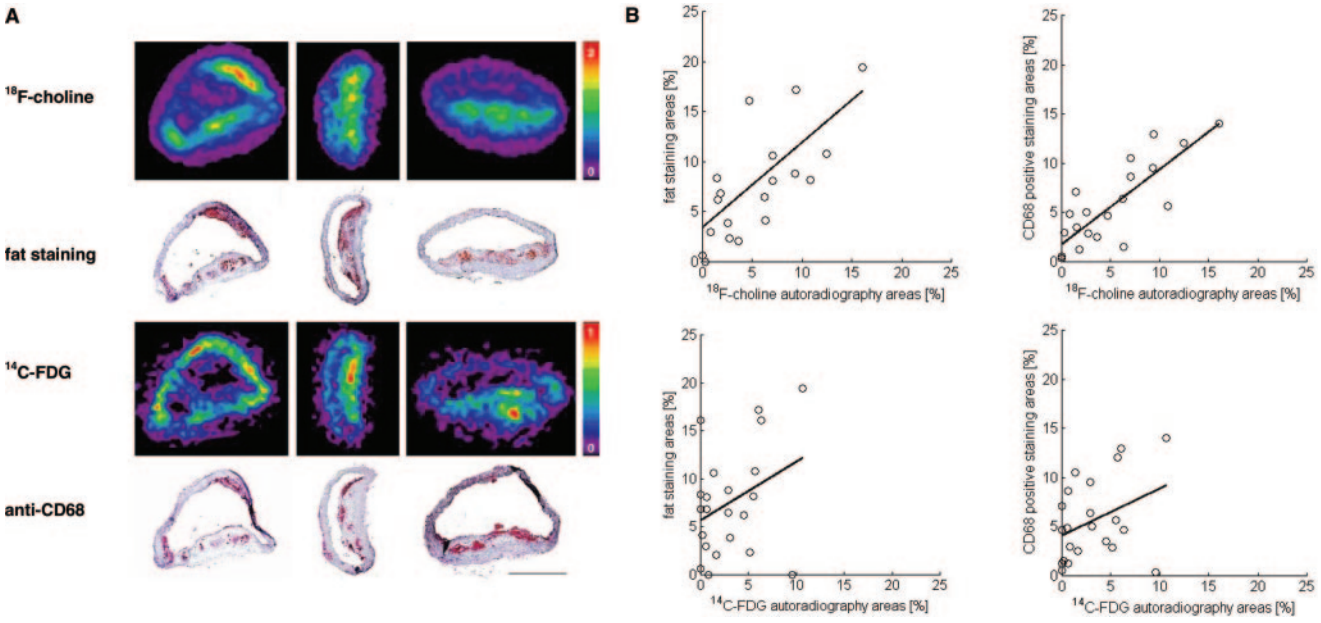

Figure 3. ^{18}F-FCH correlates with plaque macrophages. A, Aortic cross-sections after coinjections of ^{18}F-FCH and ^{14}C-FDG into the same *ApoE*$^{-/-}$ mice were exposed over 4 hours (^{18}F-FCH uptake), then re-exposed for 10 days (^{14}C-FDG uptake) followed by fat staining. Anti-CD68 stainings identified macrophages in adjacent sections. Representative photomicrographs of cross-sections from 3 different animals are shown. The color calibration (right) indicates the SUV for ^{18}F-FCH or ^{14}C-FDG, respectively; bar=500 μm. B, Uptake of ^{18}F-FCH in cross-sections (upper panel) correlates well with fat stainings (r=0.740, P<0.0001) or CD68 stainings (r=0.740, P<0.0001). ^{14}C-FDG uptake (lower panel) correlated less with fat (0.236, P=0.29) or CD68 staining (0.352, P=0.11). Each white circle (n=22) refers to a single autoradiographic signal and its corresponding fat or CD68 staining.

Staining of adjacent cross-sections for macrophages using an anti-CD68 antibody (Figure 3A, bottom) revealed that ^{18}F-FCH uptake correlated better with fat staining (r=0.740, P<0.0001) and CD68 positive areas (r=0.740, P<0.0001; Figure 3B, top; Table) than ^{14}C-FDG (fat: 0.236, P=0.29 and CD68 staining: 0.352, P=0.11; Figure 3B, bottom), respectively.

^{18}F-FCH Mouse PET

Mouse PET scans obtained 10 to 30 minutes after ^{18}F-FCH injections could not detect a specific tracer uptake in atherosclerotic aortae of *ApoE*$^{-/-}$ mice but showed an increased unspecific ^{18}F-FCH uptake in metabolically active tissues such as heart and liver. Subsequent en face analyses of these aortae revealed a good colocalization of autoradiographies and fat stainings.

Choline Kinase Expression and Activity Are Unchanged in Atherosclerotic Versus Normal Aortae

As an increased choline uptake in tumor cells has been related to an upregulation of choline kinase and/or choline transport mechanisms,[17,19] we compared expression and activity of choline kinase in atherosclerotic versus normal aortae isolated from *ApoE*$^{-/-}$ or wild-type mice, respectively. Both choline kinase expression and activity were similar. No methods are currently available for investigating choline transport in vivo.

Discussion

It is now well-recognized that plaque formation is a complex, noncontinuous process and that plaque rupture is not just a matter of size (ie, morphology), but mainly the consequence of plaque vulnerability (ie, biology). Thus, imaging of vulnerable plaques constitutes a great need in cardiovascular medicine.[5]

In this study, we describe for the first time to our knowledge ^{18}F-FCH as a promising agent for imaging biological properties of murine atherosclerotic plaques using ex vivo macroautoradiography and microautoradiography. At the cellular level, uptake of ^{18}F-FCH correlated significantly with plaque macrophages. These findings extend our previous studies in which we described ^{18}F-FCH for noninvasive imaging of a soft tissue infection in a rat model.[20]

Activated macrophages have been shown to play a key role in promoting atherogenesis. For example, by infiltrating the intimal layer, they replicate, become foam cells, and express and secrete hazardous inflammatory molecules within the arterial wall. Particularly, their formation of enzymes such as matrix metalloproteinases (MMPs) leads to thinning of the fibrous cap, thereby increasing the vulnerability of plaques.[12,13]

Enhanced ^{18}F-FDG uptake was recently reported in plaques of atherosclerotic rabbits[9] and humans.[8,10,11] Furthermore, increased ^{18}F-FDG uptake in unstable plaques colocalized with plaque macrophages,[8] suggesting increased metabolic activity. Thus, these authors proposed enhanced ^{18}F-FDG uptake in human plaques as a typical sign of plaque vulnerability. These reports and our previous findings inspired us to perform a side-by-side comparison of en face preparations 20 minutes after ^{18}F-FCH or ^{18}F-FDG injections complemented by cross-sections after simultaneous injections of ^{18}F-FCH and ^{14}C-FDG into *ApoE*$^{-/-}$ mice. As image acquisition 3

hours after ^{18}F-FDG injection was identified as the optimal time point for visualizing human vulnerable plaques via PET-CT,[8] we also investigated ex vivo imaging of murine plaques 3 hours after ^{18}F-FDG administration. Our macroscopic en face measurements demonstrated that uptake of FCH visualizes murine plaques more specifically than FDG 20 minutes or 3 hours after radiotracer injection. In particular, the sensitivity for detecting plaques ex vivo was best for ^{18}F-FCH, lower for ^{18}F-FDG at 20 minutes, and lowest 3 hours after ^{18}F-FDG at injection. In addition, our histological analyses revealed that ^{18}F-FCH uptake correlated significantly with fat and macrophage stainings better than the corresponding correlations of ^{14}C-FDG uptake. These macroautoradiographic and microautoradiographic findings suggest that FCH may even be better than FDG for visualizing murine plaques ex vivo and render ^{18}F-FCH a promising candidate for noninvasive imaging of plaque metabolism.

To be applicable for noninvasive plaque imaging, the radiolabeled particles not only have to accumulate within the target tissue, they also have to be cleared quickly from the circulating blood to provide a sufficient signal-to-noise ratio for scintigraphy or PET imaging. For this purpose, ^{18}F-FCH appears a suitable and promising tool given its rapid blood clearance rate.[23] However, our ^{18}F-FCH PET scans of *ApoE*$^{-/-}$ mice did not allow us to detect a plaque-specific signal. We think that this was caused by: (1) the difficulty to relate the PET signal to a specific anatomic structure; (2) the limited spatial resolution of small animal PET ($\approx$1 mm) to detect even smaller murine plaques ($\approx$200 to 500 μm); (3) the unspecific uptake of ^{18}F-FCH in metabolically active tissues such as liver and heart; and (4) the moderate SUV of ^{18}F-FCH as suggested by our experiments. However, we speculate that human plaque imaging using ^{18}F-FCH is feasible because of: (1) the opportunity to create hybrid images by combining high spatial resolution morphological imaging using CT or MRI with PET; (2) the considerably bigger size of human compared with murine plaques; (3) the similar SUV for ^{18}F-FDG and ^{18}F-FCH; and (4) the feasibility of human plaque imaging using ^{18}F-FDG.[8]

Radiolabeled choline is known as a proliferation marker and has been used for imaging brain and prostate cancer.[14,15] The increased choline uptake in highly proliferative cells such as tumor cells has been related to an upregulation of choline kinase as well as an increased activity of choline-specific transporters.[19,24] We show similar levels of choline kinase expression and activity in normal and atherosclerotic murine aortae. Thus, enhanced ^{18}F-FCH uptake in activated murine plaque macrophages is not caused by changes in choline kinase, but rather by increased choline transport. The rapid uptake (within 30 minutes) of ^{18}F-FCH into prostate cancer[14,15] or inflammatory tissues[20] supports this notion. Interestingly, choline and FCH are trapped in the cells, whereas the nonmetabolizable choline analogue ^{18}F-deshydroxy-FCH, which also uses the specific transport system, is weakly incorporated in the cells.[24] Thus, accumulation of FCH 20 minutes after injection in our study suggests a specific uptake, because nonspecific transport would not lead to intracellular radiotracer accumulation.

Other radionuclide-based approaches for imaging plaque biology have been reported using radiotracers such as technetium (^{99m}Tc)-linked, Indium (^{111}In)-linked, or iodine (^{125}I, ^{131}I)-linked compounds.[7] Many of the previous studies used macrophage labeling to characterize one important aspect of plaque vulnerability.[25] For example, ^{99m}Tc-labeled Annexin V visualized apoptotic macrophages in plaques of atherosclerotic rabbits[26] and in a small number of patients.[27] Similarly, uptake of ^{125}I-linked monocyte chemoattractant protein 1 (MCP-1) revealed an excellent correlation with macrophages in aortic plaques of atherosclerotic rabbits.[28] Schäfers et al recently reported on scintigraphic imaging of matrix metalloproteinase (MMP) activity in ligation-induced and cholesterol-induced carotid lesions of *ApoE*$^{-/-}$ mice using a ^{123}I-labeled MMP inhibitor.[29] Similar to our results, the radiotracer signal in these lesions colocalized with activated macrophages. However, the impact of these findings with regard to imaging of murine atherosclerotic plaques has to be interpreted with caution as the type of lesions after complete carotid ligation[30] is different from atherosclerotic plaques in terms of pathophysiology, cellular contents, and size.

Overall, given its limited spatial resolution, scintigraphic imaging using single-photon emission CT (SPECT) may severely limit the detection of small plaques. When compared with SPECT, PET is superior in terms of image resolution (4 mm versus 10 mm) and sensitivity. Although even PET-based devices do not have the spatial resolution to provide detailed tissue characterization, the lesions can be detected if there is a sufficiently high target-to-background ratio. Furthermore, the limited spatial resolution can be addressed by hybrid imaging, which combines radionuclide-based visualization of plaque biology with imaging modalities that provide better anatomic detail such as multislice CT[2] or MRI.[31] For example, PET-CT has been applied successfully at our institution for staging lung cancer[32] or assessing myocardial perfusion.[33] As mentioned, PET-CT has also been used for imaging plaque metabolism using ^{18}F-FDG.[8] Unfortunately, FDG and FCH are taken up into other metabolically active tissues such as myocardium or liver, a problem that currently excludes its use for imaging coronary atherosclerosis. Finally, the advent of catheter-based devices may provide an attractive tool for invasive detection of plaques.[34] The proximity of the β-probe close to the target is likely to improve the detection of plaque-associated radioactive signals. Combining this approach with high-resolution morphological imaging such as OCT[4] would offer an attractive technique for detailed imaging of plaque biology.

In conclusion, our findings characterize ^{18}F-FCH as a novel agent for imaging relevant aspects of plaque biology. Its colocalization with plaque macrophages may render it an additional marker of vascular inflammation suggesting vulnerability of an atherosclerotic plaque. Its favorable pharmacokinetics with rapid blood clearance as well as the opportunity to visualize ^{18}F-FCH noninvasively by PET-CT may render this approach an attractive tool for risk stratification of atherosclerotic lesions in patients.

Acknowledgments

This work was funded in part by grants from the European Union G5RD-CT-2001–00532 and by Bundesamt für Bildung und Wissenschaft 02.0057 (C.M.M., T.F.L.), the Hartmann-Müller Foundation (C.M.M., T.v.L.), the Swiss National Science Foundation 3100-068118 (T.F.L., C.M.M.), PP00A-68835 & 3100-68386.02 (P.A.K.), the Swiss Heart Foundation (P.A.K., A.B., C.M.M.), Sassella and Olga Mayenberg Foundation (A.B.), the Spanish MSC grant FIS C03-08 (J.C.L., A.R.d.M.), as well as support by Abbott/Jomed, Germany (C.M.M). We thank Tibor Cservenvàk and Rolf Hesselmann for radiotracer production.

References

1. Nair A, Kuban BD, Tuzcu EM, Schoenhagen P, Nissen SE, Vince DG. Coronary plaque classification with intravascular ultrasound radiofrequency data analysis. *Circulation*. 2002;106:2200–2206.
2. Viles-Gonzalez JF, Poon M, Sanz J, Rius T, Nikolaou K, Fayad ZA, Fuster V, Badimon JJ. In vivo 16-slice, multidetector-row computed tomography for the assessment of experimental atherosclerosis: comparison with magnetic resonance imaging and histopathology. *Circulation*. 2004;110:1467–1472.
3. Takaya N, Yuan C, Chu B, Saam T, Polissar NL, Jarvik GP, Isaac C, McDonough J, Natiello C, Small R, Ferguson MS, Hatsukami TS. Presence of intraplaque hemorrhage stimulates progression of carotid atherosclerotic plaques: a high-resolution magnetic resonance imaging study. *Circulation*. 2005;111:2768–2775.
4. Tearney GJ, Yabushita H, Houser SL, Aretz HT, Jang IK, Schlendorf KH, Kauffman CR, Shishkov M, Halpern EF, Bouma BE. Quantification of macrophage content in atherosclerotic plaques by optical coherence tomography. *Circulation*. 2003;107:113–119.
5. Choudhury RP, Fuster V, Fayad ZA. Molecular, cellular and functional imaging of atherothrombosis. *Nat Rev Drug Discov*. 2004;3:913–925.
6. Jaffer FA, Weissleder R. Seeing within: molecular imaging of the cardiovascular system. *Circ Res*. 2004;94:433–445.
7. Davies JR, Rudd JF, Fryer TD, Weissberg PL. Targeting the vulnerable plaque: the evolving role of nuclear imaging. *J Nucl Cardiol*. 2005;12:234–246.
8. Rudd JH, Warburton EA, Fryer TD, Jones HA, Clark JC, Antoun N, Johnstrom P, Davenport AP, Kirkpatrick PJ, Arch BN, Pickard JD, Weissberg PL. Imaging atherosclerotic plaque inflammation with [18F]-fluorodeoxyglucose positron emission tomography. *Circulation*. 2002;105:2708–2711.
9. Ogawa M, Ishino S, Mukai T, Asano D, Teramoto N, Watabe H, Kudomi N, Shiomi M, Magata Y, Iida H, Saji H. (18)F-FDG accumulation in atherosclerotic plaques: immunohistochemical and PET imaging study. *J Nucl Med*. 2004;45:1245–1250.
10. Ben-Haim S, Kupzov E, Tamir A, Israel O. Evaluation of 18F-FDG uptake and arterial wall calcifications using 18F-FDG PET/CT. *J Nucl Med*. 2004;45:1816–1821.
11. Tatsumi M, Cohade C, Nakamoto Y, Wahl RL. Fluorodeoxyglucose uptake in the aortic wall at PET/CT: possible finding for active atherosclerosis. *Radiology*. 2003;229:831–837.
12. Ross R. Atherosclerosis–an inflammatory disease. *N Engl J Med*. 1999;340:115–126.
13. Glass CK, Witztum JL. Atherosclerosis. the road ahead. *Cell*. 2001;104:503–516.
14. Yoshimoto M, Waki A, Obata A, Furukawa T, Yonekura Y, Fujibayashi Y. Radiolabeled choline as a proliferation marker: comparison with radiolabeled acetate. *Nucl Med Biol*. 2004;31:859–865.
15. Schmid DT, John H, Zweifel R, Cservenyak T, Westera G, Goerres GW, von Schulthess GK, Hany TF. Fluorocholine PET/CT in Patients with Prostate Cancer: Initial Experience. *Radiology*. 2005;235:623–628.
16. Haeffner EW. Studies on choline permeation through the plasma membrane and its incorporation into phosphatidyl choline of Ehrlich-Lettre-ascites tumor cells in vitro. *Eur J Biochem*. 1975;51:219–228.
17. Boggs KP, Rock CO, Jackowski S. Lysophosphatidylcholine and 1-O-octadecyl-2-O-methyl-rac-glycero-3-phosphocholine inhibit the CDP-choline pathway of phosphatidylcholine synthesis at the CTP: phosphocholine cytidylyltransferase step. *J Biol Chem*. 1995;270:7757–7764.
18. Katz-Brull R, Degani H. Kinetics of choline transport and phosphorylation in human breast cancer cells; NMR application of the zero trans method. *Anticancer Res*. 1996;16:1375–1380.
19. Ramirez de Molina A, Gutierrez R, Ramos MA, Silva JM, Silva J, Bonilla F, Sanchez JJ, Lacal JC. Increased choline kinase activity in human breast carcinomas: clinical evidence for a potential novel antitumor strategy. *Oncogene*. 2002;21:4317–4322.
20. Wyss MT, Weber B, Honer M, Spath N, Ametamey SM, Westera G, Bode B, Kaim AH, Buck A. 18F-choline in experimental soft tissue infection assessed with autoradiography and high-resolution PET. *Eur J Nucl Med Mol Imaging*. 2004;31:312–316.
21. Spaeth N, Wyss MT, Weber B, Scheidegger S, Lutz A, Verwey J, Radovanovic I, Pahnke J, Wild D, Westera G, Weishaupt D, Hermann DM, Kaser-Hotz B, Aguzzi A, Buck A. Uptake of 18F-fluorocholine, 18F-fluoroethyl-L-tyrosine, and 18F-FDG in acute cerebral radiation injury in the rat: implications for separation of radiation necrosis from tumor recurrence. *J Nucl Med*. 2004;45:1931–1938.
22. Plump AS, Smith JD, Hayek T, Aalto-Setala K, Walsh A, Verstuyft JG, Rubin EM, Breslow JL. Severe hypercholesterolemia and atherosclerosis in apolipoprotein E- deficient mice created by homologous recombination in ES cells. *Cell*. 1992;71:343–353.
23. DeGrado TR, Coleman RE, Wang S, Baldwin SW, Orr MD, Robertson CN, Polascik TJ, Price DT. Synthesis and evaluation of 18F-labeled choline as an oncologic tracer for positron emission tomography: initial findings in prostate cancer. *Cancer Res*. 2001;61:110–117.
24. Henriksen G, Herz M, Hauser A, Schwaiger M, Wester HJ. Synthesis and preclinical evaluation of the choline transport tracer deshydroxy-[18F]fluorocholine ([18F]dOC). *Nucl Med Biol*. 2004;31:851–858.
25. Schaar JA, Muller JE, Falk E, Virmani R, Fuster V, Serruys PW, Colombo A, Stefanadis C, Ward Casscells S, Moreno PR, Maseri A, van der Steen AF. Terminology for high-risk and vulnerable coronary artery plaques. Report of a meeting on the vulnerable plaque, June 17 and 18, 2003, Santorini, Greece. *Eur Heart J*. 2004;25:1077–1082.
26. Kolodgie FD, Petrov A, Virmani R, Narula N, Verjans JW, Weber DK, Hartung D, Steinmetz N, Vanderheyden JL, Vannan MA, Gold HK, Reutelingsperger CP, Hofstra L, Narula J. Targeting of apoptotic macrophages and experimental atheroma with radiolabeled annexin V: a technique with potential for noninvasive imaging of vulnerable plaque. *Circulation*. 2003;108:3134–3139.
27. Kietselaer BL, Hofstra L, Dumont EA, Reutelingsperger CP, Heidendal GA. The role of labeled Annexin A5 in imaging of programmed cell death. From animal to clinical imaging. *Q J Nucl Med*. 2003;47:349–361.
28. Ohtsuki K, Hayase M, Akashi K, Kopiwoda S, Strauss HW. Detection of monocyte chemoattractant protein-1 receptor expression in experimental atherosclerotic lesions: an autoradiographic study. *Circulation*. 2001;104:203–208.
29. Schafers M, Riemann B, Kopka K, Breyholz HJ, Wagner S, Schafers KP, Law MP, Schober O, Levkau B. Scintigraphic imaging of matrix metalloproteinase activity in the arterial wall in vivo. *Circulation*. 2004;109:2554–2559.
30. Kumar A, Lindner V. Remodeling with neointima formation in the mouse carotid artery after cessation of blood flow. *Arterioscler Thromb Vasc Biol*. 1997;17:2238–2244.
31. Toussaint JF, LaMuraglia GM, Southern JF, Fuster V, Kantor HL. Magnetic resonance images lipid, fibrous, calcified, hemorrhagic, and thrombotic components of human atherosclerosis in vivo. *Circulation*. 1996;94:932–938.
32. Lardinois D, Weder W, Hany TF, Kamel EM, Korom S, Seifert B, von Schulthess GK, Steinert HC. Staging of non-small-cell lung cancer with integrated positron-emission tomography and computed tomography. *N Engl J Med*. 2003;348:2500–2507.
33. Koepfli P, Hany TF, Wyss CA, Namdar M, Burger C, Konstantinidis AV, Berthold T, Von Schulthess GK, Kaufmann PA. CT attenuation correction for myocardial perfusion quantification using a PET/CT hybrid scanner. *J Nucl Med*. 2004;45:537–542.
34. Lederman RJ, Raylman RR, Fisher SJ, Kison PV, San H, Nabel EG, Wahl RL. Detection of atherosclerosis using a novel positron-sensitive probe and 18-fluorodeoxyglucose (FDG). *Nucl Med Commun*. 2001;22:747–753.

^{18}F-Choline Images Murine Atherosclerotic Plaques *ex vivo* – Supplemental Online Material

Materials and Methods

Animals

Male atherosclerotic apolipoprotein E knockout (*ApoE*$^{-/-}$, C57Bl/6J) mice [1] were obtained from Jackson Laboratories (Bar Harbor, ME, USA) and bred at our institution. These animals were fed a high-cholesterol diet (1.25% total cholesterol, RD12108 from Research Diets, USA) for 2 months starting at the age of 8 weeks. Animals were kept without food for 4 hours prior to injections of the radiotracers until sacrifice. A subset of wild-type C57Bl/6J mice without atherosclerosis received a normal chow diet. They were used as control animals for biochemical analyses. All animal experiments were performed in accordance with our institutional guidelines and approved by the local animal committee.

Radionuclides

Ex vivo plaque imaging was performed following intravenous (i.v.) injections of ^{18}F-FCH (45.8–60.5 MBq; n=5), ^{18}F-FDG (36.7–46.4 MBq; n=5) or coinjections of ^{18}F-FCH and ^{14}C-FDG (185kBq; n=3) in 300µl normal saline into the animal's tail vein.

Harvesting and tissue processing

For determining the uptake of ^{18}F-FCH, ^{18}F-FDG or ^{14}C-FDG within plaques, *ApoE*$^{-/-}$ mice were sacrificed 20 minutes after injection of the radiotracer(s); additional animals were euthanized 3 hours after ^{18}F-FDG injections. After puncturing the left ventricle and cutting the right atrium, vessels were rinsed briefly with normal saline and the aorta excised after removing adventitial tissue. For en face analyses, distal aortae (from the left subclavian artery to the iliac bifurcation) were opened longitudinally. For microscopic examinations, 3 samples of the proximal aorta (ascending, mid and distal arch) were embedded in OCT compound (Tissue-Tek, Sakura, The Netherlands) and frozen in isopentane. Serial cross sections of 10µm thickness (at 100µm intervals) were immediately cut and thaw-mounted on glass slides. Autoradiography and fat stainings were performed on the same samples (n=12 from each animal).

Adjacent cross sections were saved for immunohistochemistry. For biochemical analyses, aortae from *ApoE*$^{-/-}$ (n=3) and wild-type mice (n=3) were shock-frozen in liquid nitrogen and stored at -80°C.

Choline kinase activity and expression

For tissue extracts, samples were homogenized in buffer containing 1.5mM $MgCl_2$, 0.2mM EDTA, 0.3M NaCl 25mM HEPES pH 7.5, 20mM β-glycerophosphate and 0.1% TRITON X-100. Choline kinase (CHK) assays were performed from homogenized tissues in buffer containing 100mM Tris-HCl pH 8.0, 100mM $MgCl_2$ and 10mM ATP. Physiological choline concentration (200μM) was used as substrate in the presence of methyl[^{14}C]-choline chloride (50-60Ci/mmol, Amersham International). Reactions were performed at 37°C for 30 minutes and stopped with ice cold 16% trichloracetic acid. Hydrophylic derivatives of choline (i.e. phosphorylcholine) were resolved by thin layer chromatography plates (60 A silica gel, Whatman, Clifton, NJ) using as liquid phase 0.9% NaCl: methanol: ammonium hydroxide (50:70:5; V:V:V). Radioactivity corresponding to *P*-Choline was quantified by an electronic radiography system (Instantimager; Packard, Meriden, CT). Equal amounts of protein (30μg) from the different tissue lysates were used for Western blot analysis using a monoclonal antibody raised against human choline kinase α that also recognizes mouse choline kinase (Gallego-Ortega et al., unpublished data, 2005) and then developed by ECL as described by the manufactures (Amersham). α-tubulin (T9026, Sigma) was used as a loading control.

Plaque imaging

Plaque imaging was performed *ex vivo* in 3 dimensions by combining macroscopic measurements of en face preparations of the thoraco-abdominal aorta with microscopic analyses of cross-sections of the proximal aorta.

Morphology: Plaque areas were assessed via fat staining using Oil-red O. Macrophages were identified using a rat anti-mouse CD68 monoclonal antibody (Serotec, Clone FA-II, 1:400), a goat anti-rat secondary antibody (IgG, Caltag R40000, 1:150) followed by an alkaline phosphatase-conjugated donkey anti-goat antibody (IgG, Jackson 705-055-147, 1:80). Sections were counterstained with hematoxyline.

Autoradiography: Two different methods were employed in order to assess tracer uptake. For en face autoradiography, aortae were longitudinally opened and exposed on a phosphor imaging screen with ^{14}C standards (for 4 hours with ^{18}F-labeling – for 10d using ^{14}C labeling). Furthermore, aortic cross-sections of 10µm thickness were exposed with ^{14}C standards for microautoradiography. The data were scanned (Fuji BAS 1800 II, pixel size: 50µm) and converted to kBq/cc. For this conversion, the ^{14}C standards were previously recalibrated using a 4-hour exposure of 10µm slices of a brain homogenate containing a defined amount of ^{18}F activity.

Signal quantifications: The lesion-to-nonlesion ratio in autoradiographies of longitudinally opened aortae was determined using linear integration of signal intensity (NIH Image J 1.33 software) over corresponding aortic areas taking the mean of 5 measurements from each animal. The corresponding ratio in 3 cross-sections of the proximal aorta was determined after injections of ^{18}F-FCH or ^{18}F-FDG by relating the signal intensity of an area of interest within the plaque to an area without lesion. In addition, the standardized uptake value (SUV) was obtained for each animal by dividing the target tissue radioactivity uptake (kBq/cc) within a region of interest by the injected activity per gram of body weight. Comparisons between en face fat stainings and corresponding autoradiographies were determined by converting the autoradiographies into color-coded images using the software PMOD [2], tracing all positive areas (Analysis Five Docu, Software from SoftImaging System) and correlating the % positive out of the total vessel areas using the Spearman rank correlation test (GraphPad Prism V4). Similar comparisons were performed from 3 aortic cross sections after coinjections of ^{18}F-FCH and ^{14}C-FDG (n=3) for autoradiographies, fat and CD68 stainings. For all above mentioned calculations, multiple plaques on the aorta of one animal were considered independent samples; 0 values were inserted with absence of a corresponding value of either plaques or autoradiographies.

Mouse Positron Emission Tomography (PET): PET experiments were performed on the 16-module variant of the NanoPET™ tomograph (Oxford Positron Systems; Weston-on-the-Green, UK) as described [3]. PET scans were obtained 10 to 30 min after intravenous ^{18}F-FCH (18.62–19.63) injections in atherosclerotic *ApoE*$^{-/-}$ mice (n=3). Harvestings of aortae for en face analyses were performed 40 minutes after the radiotracer injections.

Statistics

An unpaired t-test was used to compare results between different groups. Values are given as mean±SD; $P<0.05$ was considered statistically significant.

Figures and Table

Figure I

A

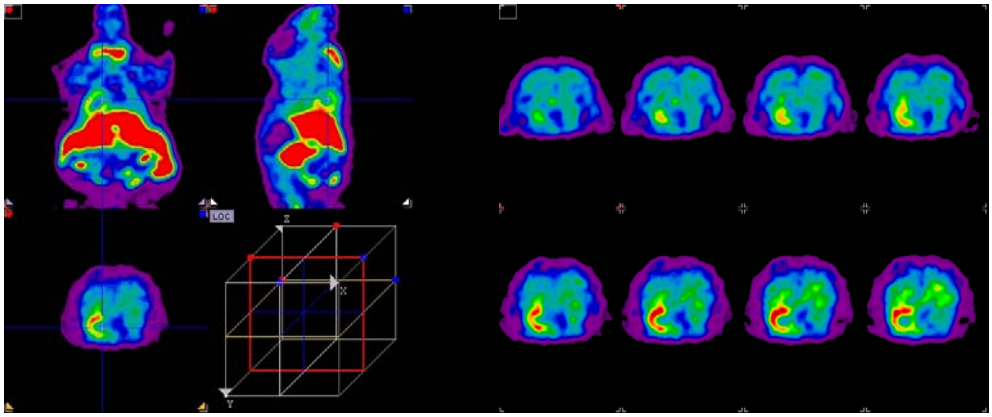

B

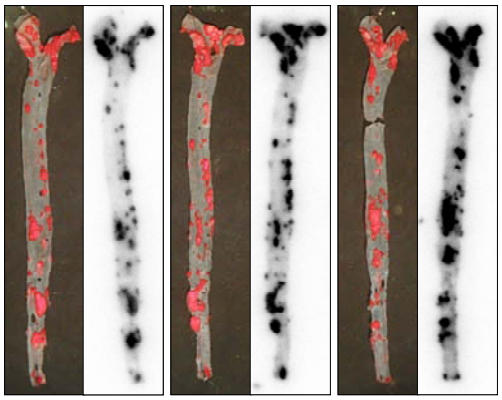

Figure I: PET scans and ex vivo autoradiographies after ^{18}F-choline injections.

(**A**) PET scans obtained 10 to 30 min after intravenous ^{18}F-FCH (18.62–19.63 MBq, n=3) injections did not allow to detect a specific tracer uptake in plaques of atherosclerotic aortae of *ApoE*$^{-/-}$ mice, but showed an increased ^{18}F-FCH uptake in metabolically active tissues such as heart and liver. Left panel: above left: frontal plane, above right: sagittal plane; bottom left: horizontal plane; right panel: cross sections from cranial (top) to caudal (bottom). (**B**) Subsequent en face analyses of atherosclerotic aortae 40 minutes after ^{18}F-FCH injection revealed a good colocalization of autoradiographies (right) and fat stainings (left).

Figure II

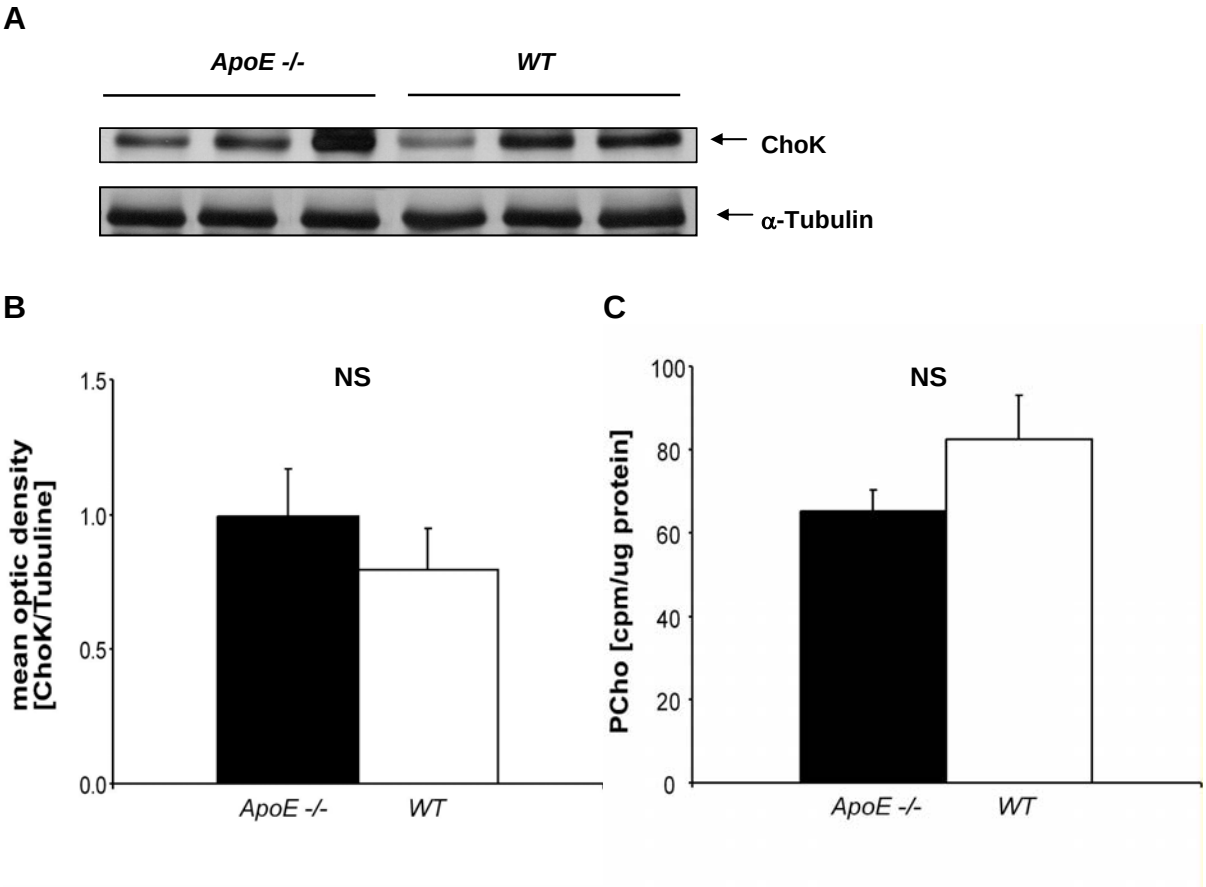

Figure II. Similar choline kinase expression and activity in atherosclerotic and normal murine aortae.

Analysis of aortic lysates from atherosclerotic *ApoE*$^{-/-}$ (n=3) or normal wild-type (WT, n=3) mice reveal similar choline kinase (ChoK) expression by Western blotting (**A**) and subsequent densitometric quantifications (NS, **B**). In parallel, choline kinase activity measured by the amount of phospho-choline (PCho; **C**) was not different in lysates obtained from atherosclerotic (n=3) or normal (n=3) aortae (n=3, NS).

Table I. Validation of ^{18}F-FCH or ^{18}F FDG for imaging murine plaques *ex vivo* en face.

Radiotracer (time interval)	**^{18}F-FCH (20min)**	**^{18}F-FDG (20min)**	**^{18}F-FDG (3h)**
n (mice)	5	5	3
n (total plaques analyzed en face)	89	73	58
Correlation r (Spearman)	0.842	0.261	0.476
P value (Spearman)	<0.0001	<0.05	<0.001
False negative autoradiography (%)	19	51	76
Sensitivity of tracer for plaque imaging (%)	84	64	57
Signal-to-noise (plaque-to-nonlesion)	4.9±2.0 to 1	6.0±5.1 to 1	2.6±0.9 to 1

Comparisons of single autoradiographic signals and fat stainings in longitudinally opened atherosclerotic aortae; mean±SD.

References

1. Plump AS, Smith JD, Hayek T, Aalto-Setala K, Walsh A, Verstuyft JG, Rubin EM, Breslow JL. Severe hypercholesterolemia and atherosclerosis in apolipoprotein E- deficient mice created by homologous recombination in ES cells. *Cell.* 1992;71:343-353.
2. Mikolajczyk K, Szabatin M, Rudnicki P, Grodzki M, Burger C. A JAVA environment for medical image data analysis: initial application for brain PET quantitation. *Med Inform (Lond).* 1998;23:207-214.
3. Missimer J, Madi Z, Honer M, Keller C, Schubiger A, Ametamey SM. Performance evaluation of the 16-module quad-HIDAC small animal PET camera. *Phys Med Biol.* 2004;49:2069-2081.